Identification of PKN2 and MOB4 as Coordinators of Collective Cell Migration

Artem I. Fokin[1,2], Yueying Lin[3], Dmitry Y. Guschin[1,*], Hsiang-Ying Chen[2], John James[1], Jie Yan[3,4], Pascal Silberzan[2§], Alexis M. Gautreau[1§]

[1] Laboratoire de Biologie Structurale de la Cellule (BIOC), CNRS, École Polytechnique, Institut Polytechnique de Paris, 91120 Palaiseau, France

[2] Institut Curie, Université PSL, Sorbonne Université, CNRS UMR168, Physique des Cellules et Cancer, 75005 Paris, France

[3] Mechanobiology Institute, National University of Singapore, Singapore 117411, Singapore

[4] Department of Physics, National University of Singapore, Singapore 117542, Singapore

[*] Present address: Scientific Center for Translational Medicine, Sirius University of Science and Technology. 254349 Sirius, Russian Federation.

[§] Corresponding authors:

pascal.silberzan@curie.fr

alexis.gautreau@polytechnique.edu

ABSTRACT

In animals, collective cell migration is critical during development and adult life for repairing organs. It remains, however, poorly understood compared with single cell migration. Polymerization of branched actin by the RAC1-WAVE-Arp2/3 pathway is well established to power membrane protrusions at the front of migrating cells, but also to maintain cell junctions in epithelial monolayers. Here we performed a screen for novel regulators of collective cell migration by identifying genes associated with the RAC1-WAVE-Arp2/3 pathway at cell junctions using dependency maps and by inactivating these candidates using CRISPR/Cas9. In wound healing, MCF10A epithelial cells collectively migrate towards the free space in a coordinated manner. PKN2 knockout (KO) cells display decreased collective migration due to destabilization of adherens junctions, whereas MOB4 KO cells display increased collective migration with a swirling behavior. Upon wound healing, PKN2 relocalizes to lateral junctions and maintains coordinated migration in the monolayer, whereas MOB4 relocalizes to the front edge of cells migrating towards the wound. The role of MOB4 in controlling collective migration requires YAP1, since MOB4 KO cells fail to activate YAP1 and their phenotype is rescued by constitutively active YAP1. Together, our data reveal two complementary activities required for coordinating cells in collective migration.

Keywords: PKN2, MOB4, WAVE complex, E-cadherin, YAP1.

1. INTRODUCTION

Collective cell migration is essential to the development and adult life of animals, starting from gastrulation, continuing later on during organogenesis and healing of injuries throughout life [1]. It is also important for pathological processes, such as cancer progression and tumor cell invasion [2]. Collective cell migration displays similarities with single cell migration. For example, leader cells develop an adherent membrane protrusion at their front called a lamellipodium, like single migrating cells [3,4]. However, all collectively migrating cells, including follower cells, develop such a lamellipodium, even if they do not have a free edge and thus their lamellipodium it is hidden by the cell located immediately ahead. It is then referred to as a cryptic lamellipodium [5–8].

Lamellipodia are the results of the pushing force exerted by the polymerization of branched actin through the Arp2/3 complex [9,10]. However, cortical branched actin also pushes against the cell-cell junctions of epithelial cells and this activity has been demonstrated to be critical for the establishment and maintenance of adherens junctions [11–13] . In fact, at cell-cell junctions, there is a balance of pulling forces due to myosin mediated contractility on linear arrays of actin filaments and of Arp2/3 branched arrays pushing and affixing membranes of neighboring cells, thus allowing cells to re-establish adherens junctions after excessive contractility might have induced a bulge between neighboring cells [14,15]. Strikingly the same pathway that involves a sequential activation of the small GTPase RAC1, the WAVE nucleation promoting factor and Arp2/3, is involved in forming membrane protrusions at the free edge of migrating cells and at cell-cell junctions of epithelial cells [16,17]. This implies that the same molecular mechanism of branched actin generation might be differentially regulated at these two locations. But how this differential regulation is achieved is currently not known.

In collective cell migration, coordination of cells involves cell-cell junctions [18,19]. In a fully confluent monolayer, epithelial cells stop migrating in a process known as jamming [20] . Unjamming can, however, occur at the same high cell density upon endocytic control of E-cadherin trafficking and adherens junctions [21]. When collective migration is directed, as in wound healing, migration orientation is mechanotransduced across cell-cell junctions, from leader cells facing the wound to follower cells [22]. The mechanotransducer vinculin that connects actin filaments to integrin-mediated focal adhesions also connects actin filaments to E-cadherin-mediated adherens junctions [23]. The NF2 tumor suppressor, which is associated with cell-cell junctions in a jammed epithelium and relocalizes to the cytosol upon unjamming, appears to transmit wound sensing into activation of the GTPase RAC1 and the YAP1 transcription factor [24,25]. In wound healing, the mechanosensitive YAP1 is activated in cells facing the wound and induce the expression of genes associated with proliferation and adhesion [26–28].

To gain insights into the mechanisms of cell coordination in collective migration, we conducted a two-step genetic screen using the RAC1-WAVE-Arp2/3 as an entry point, since this pathway is involved in establishing and maintaining lamellipodial protrusions and cell junctions. We identified two previously unknown regulators of cell migration: PKN2 that maintains epithelial cohesiveness in collectively migrating cells, and MOB4 that indicates the proper orientation of migration to follower cells.

2. RESULTS

2.1 Selection of Candidate Genes and Isolation of Knockout Clones

To identify novel factors connected to the RAC1-WAVE-Arp2/3 pathway, we exploited the so-called dependency maps [29]. In this approach, a library of gRNAs is transduced into a cell line and analyzed by Next Generation Sequencing (NGS), first at the time of transduction and then after 16 doublings of the cell population (Figure 1A). The comparison of the two NGS allows identifying gRNAs that are significantly depleted, corresponding to essential genes, or enriched, corresponding to tumor suppressor genes. Since the same analysis has been repeated in more than 500 cell lines, genes encoding different signaling intermediates of the same pathway are found to be essential in the same cell lines and unessential in the others. We thus explored gene correlations in the depmap.org public database and verified that the genes encoding RAC1 and several subunits of the WAVE and Arp2/3 complexes were indeed positively correlated with each other, as expected (Figure 1B). The gene encoding the mechanotransducer vinculin, which associates with Arp2/3 [30,31], was similarly correlated. In contrast, *NF2*, a tumor suppressor gene, known to antagonize the RAC1 pathway [32,33], was anti-correlated with all the above factors. These correlations confirmed that the biomechanical regulation of branched actin can be inferred from dependency maps. In addition to the core RAC1-WAVE-Arp2/3 pathway that polymerizes cortical branched actin, we found that many proteins of the integrin pathway were also encoded by correlated genes. This was, for example, the case of Kindlin-2 and Focal Adhesion Kinase, which both associate with the Arp2/3 complex [34–36]. In our focus on collective cell migration, we filtered out all candidates connected to the integrin pathway and selected candidate genes that encoded proteins physically or functionally associated with cell-cell junctions. This short list contained five candidate genes: *PKN2*, *TP53BP2*, *DLG5*, *MOB4* and *AMOTL2*.

The *PKN2* gene encodes the serine/threonine protein kinase N2, PKN2, also known as PRK2. PKN2 is an effector of both RHOA and RAC1 GTPases that regulates the formation of cell junctions [37,38]. PKN2 was found in the E-cadherin interactome [39]. The *TP53BP2* gene encodes a p53 binding protein, TP53BP2, which is also known as ASPP2. TP53BP2 binds to E-cadherin and β-catenin and regulates epithelial to mesenchymal transition (EMT) [40]. TP53BP2 also associates with the tumor suppressor NF2 [41]. TP53BP2 maintains the integrity of stressed epithelia and inhibits cell migration and proliferation [42,43]. *DLG5* encodes the adapter protein Disks large homologue 5, a conserved member of the MAGUK family. DLG5 interacts with β-catenin [44] and maintains the integrity of epithelial monolayers [45]. DLG5 depletion induces EMT and increases cell migration and proliferation [46,47]. *MOB4* encodes a protein of the phocein family. MOB4 regulates the mechanosensitive YAP1 pathway by associating with the MST4 kinase [48] and contributes to a large assembly containing the PP2A phosphatase called the STRIPAK complex [49,50]. The negatively correlated gene *AMOTL2*, which can be an oncogene or tumor suppressor depending on the cancer

[51,52] encodes an Angiomotin family protein. AMOTL2 localizes to cell-cell junctions and regulates the NF2 tumor suppressive activity [53].

For fast and efficient knock-out (KO) of these candidate genes, we combined purified Cas9 protein with three synthetic gRNAs: two that introduce double-strand breaks in the target gene, thus inducing a deletion, and one that targets the gene encoding the essential Na+/K+ antiporter ATP1A1 at the position of its ouabain binding site. Ouabain thus selects cells carrying mutated *ATP1A1*, where the double-strand break has been repaired by non-homologous end joining, in such a way that the antiporter was functional, but insensitive to ouabain [54]. This efficient selection renders deletion screening fast (10 to 90 % success rate) and permitted us to retrieve KO clones from the MCF10A breast epithelial cell line for each the five target genes. We selected two KO clones for each gene, whose alleles were sequenced to identify precise deletions, resulting most often in a frameshift (Figure S1). All KO clones were further validated by Western blot (Figure 1C). We compared these KO clones with parental MCF10A cells and a pool of ouabain-resistant cells.

2.2 Screening Candidate Genes for their Role in Collective Cell Migration

We then tested these KO cell lines in a model wound healing, obtained by lifting inserts to create a free area, an assay that induces collective migration of cells towards the wound [55]. Leader cells from MCF10A monolayers close the wound with a smooth progressing edge unlike MDCK cells that form so-called fingers driven by leader cells at the edge [56] . To quantitatively analyze the coordination of collectively migrating cells, we applied particle image velocimetry (PIV) to movies acquired with phase contrast [57] . The ensuing field of displacement vectors varied over time and allowed extracting two major parameters: the order parameter that reflects the migration orientation towards the wound and the speed of cells (Figure 2A) [58] . These parameters are then represented as heat maps to capture their evolution in time and space. Parental cells or ouabain-resistant controls exhibited a stereotypical response to the wound (Figure 2B, Figure S2): cells next to the wound, over about 500 μM in depth, began migrating in a coordinated manner towards the wound. Three selected genes, *DLG5*, *AMOTL2* and *TP53BP2*, appeared not to be involved in wound healing, since the corresponding KO clones behaved like controls. In sharp contrast, two of our selected genes dramatically affected cell behavior: PKN2 KO decreased both order and velocity of cells in the wounded monolayer (Video S1), whereas MOB4 KO increased velocity and extended the territory of collectively migrating cells (Video S2). Both clones of each KO behaved similarly (Figure S2). However, we realized that heat maps of each MOB4 KO field of view were unique, because these cells, which were efficiently collectively migrating over large territories, exhibited erratic changes of migration orientation (Video S3, Video S4). We refer to this striking feature as the swirling behavior of MOB4 KO cells. As a consequence, averaging several fields of view captures the overall decrease in migration parameters in PKN2 KO and the overall increase in MOB4 KO, but not the unstable directionality of MOB4 KO cells, which is best appreciated by mapping migration orientation in single fields of view (Figure 2C). MOB4 KO cells also migrated collectively for longer, until they eventually jammed at least 10 h later than control cells (Figure S3). Our miniscreen thus revealed a positive and a negative regulator of collective migration, yet both PKN2 and MOB4 KO

cells were globally less efficient at closing the wound (Figure S4), because of defective coordination in collective migration.

2.3 PKN2 and MOB4 Associate with Front or Lateral WAVE Complexes

To better understand the roles of PKN2 and MOB4, we generated stable MCF10A cell lines expressing either GFP-PKN2 or GFP-MOB4 (Figure S5). The two proteins appeared mostly cytosolic. However, in wounded monolayers, a small fraction of both proteins translocates to cell junctions in migrating cells (Video S5). The membrane pool of PKN2 and MOB4 colocalizes with WAVE2 (Figure 3A). When PKN2 and MOB4 were immunoprecipitated, a small amount of WAVE complexes was coprecipitated (Figure 3B). These results were consistent with dependency maps indicating that PKN2 and MOB4 belonged to the same pathway as WAVE complexes, but could not account for their different functions.

A closer examination of the cell junctions stained by GFP-PKN2 and GFP-MOB4 revealed that most junctions decorated with PKN2 were orthogonal to the edge, whereas most junctions decorated with MOB4 were parallel to the edge (Figure 4A). In leader cells, the closest ones to the free space of the wound, lamellipodial edges did not show any particular enrichment of MOB4. In follower cells, the ones following the leaders, hence having neighboring cells all around their periphery, the enrichment of GFP-MOB4 at junctions parallel to the edge might occur either at the front or the back of cells. To distinguish these two possibilities, we mixed GFP-MOB4 expressing cells to non-fluorescent parental cells and observed that the front of fluorescent cells was stained (Figure 4B, Video S6), indicating that MOB4 is a front marker enriched in cryptic lamellipodia crawling beneath cells located in front of them.

We then sought to confirm this striking observation using immunofluorescence of endogenous PKN2 and MOB4. Using validated antibodies that do not stain the corresponding KO cell lines (Figure S6), we indeed observed that endogenous PKN2 decorates lateral cell junctions, whereas MOB4 decorates front cell junctions (Figure 4C), like the corresponding GFP fusion proteins. Together these observations suggest that PKN2 associates with lateral WAVE complexes that maintain and repair cell junctions, whereas MOB4 associates with front WAVE complexes responsible for the cryptic lamellipodia that drive collective migration of follower cells.

2.4 PKN2 Controls Collective Migration by Maintaining Stable Cell Junctions

We noticed that PKN2 KO cells were less prone to form epithelial islets when growing in regular culture. At most, PKN2 KO cells associated as doublets, but not as islets containing more than two cells (Figure 5A). However, this phenotype was associated with lower proliferation (Video S7), providing a plausible explanation as to why islets contained fewer cells in PKN2 KO cultures. We thus blotted PKN2 KO and parental cells for E-cadherin, the major cell-cell adhesion molecule of epithelial cells, which exerts calcium-dependent homotypic interactions between neighboring cells. The E-cadherin pool was unaltered in PKN2 KO cells (Figure 5B). However, E-cadherin was not decorating cell junctions in PKN2 KO cells as in parental cells (Figure 5C). As a proxy to cell-cell

adhesion, we used a biophysical assay consisting in measuring the force by which E-cadherin coated beads interact with cells [59]. Consistent with the observed decreased pool of E-cadherin at the membrane of PKN2 KO cells, we observed decreased mechanical stability of E-cadherin coated beads with PKN2 KO cells compared with parental cells (Figure 5D).

In order to mimic this defect, we treated parental cells with EDTA that chelates Ca^{2+} ions, which are necessary for E-cadherin mediated adherens junctions, or with EDTA and Ca^{2+} to neutralize the effect of EDTA. Upon wounding, we observed that EDTA treated cells exhibited the same behavior as PKN2 KO cells: cells at the front edge detached from the monolayer and migrated as single cells (Figure 6A, Video S8). Upon Ca^{2+} replenishment, this phenotype was abolished. This experiment suggests that PKN2 KO cells display decreased coordination in collective migration, because the formation of adherens junctions is impaired.

2.5 MOB4 Controls the Orientation of Collective Migration by Activating YAP1

Since MOB4 had been described as a non-canonical regulator of the YAP1 pathway [48], we stained MOB4 KO cells and parental cells with YAP1 antibodies. Upon wounding, front cells of MCF10A cells exhibited YAP1 in the nucleus. This nuclear translocation was particularly clear in the first row of cells next to the wound and declined further back in the monolayer that remained jammed. In sharp contrast, YAP1 was not translocated in the nucleus in the first rows of cells facing the wound in MOB4 KO cells (Figure 7A). Nuclear translocation of YAP1 is antagonized by its phosphorylation, which is required for its cytosolic retention [60,61]. YAP1 was indeed more phosphorylated on residues S127 and S397 in MOB4 KO cells than in parental MCF10A cells (Figure 7B). We wondered if this defect could account for the migration phenotype of MOB4 KO cells and attempted to rescue KO cells by the expression of a constitutively active form of YAP1 that cannot be inactivated by phosphorylation, YAP1 5SA [60]. We isolated KO cells that expressed different levels of active YAP1 (Figure 7C) and submitted these new cell lines to the wound healing assay. Strikingly, expression of YAP1 5SA abolished the MOB4 KO phenotype, i.e. the increased collective migration with swirling, in a dose-dependent manner (Figure 7D-E, Video S9). Together, these results suggest that MOB4 controls collective cell migration through YAP1 activation.

3. DISCUSSION

Out of the five candidate genes that we selected, two were indeed involved in the cell coordination of collective migration. Our selective criteria of genes correlating with the RAC1-WAVE-Arp2/3 in dependency maps and being associated with cell-cell junctions thus considerably enriched for regulators of collective migration and thus allowed for a low throughput secondary validation using KO and careful analysis of velocity fields. Our approach can be compared to a previous large siRNA screen similarly performed in a wound healing assay of MCF10A cells [62]. This previous screen identified 66 positive or negative regulators of collective cell migration, out of 1081 genes tested, which included the complete sets of kinases and phosphatases of the human genome and genes identified in another screen for cell adhesion and single cell migration. Our enrichment of candidates using dependency maps thus appear superior (2/5 >> 66/1081). Interestingly, the kinase PKN2 was missed in the siRNA screen even though other genes of this class, characterized by cell detachment at the front edge of the monolayer, were identified. In contrast, the dramatic swirling behavior of MOB4 KO cells we report here was not previously reported to our knowledge, even if many negative regulators of collective migration, like MOB4, were identified in the siRNA screen.

PKN2 involvement in collective migration may appear obvious: a gene that renders epithelial cells isolated when inactivated, because of E-cadherin internalization and cell-cell junctions destabilization, should logically abrogate collective behaviors. Nonetheless, in our short list of five candidates, the three remaining proteins that did not alter collective migration, TP53BP2, AMOTL2 and DLG5, were all associated with E-cadherin and/or β-catenin at adherens junctions [40,44,63], and similar to PKN2, they favored epithelial cohesiveness since TP53BP2 prevents EMT [40], DLG5 maintains the epithelial integrity of kidney tubules [45], and AMOTL2 is required for the proper hexagonal packing of epithelial cells within monolayers [63]. These roughly similar functions must be exerted in different cellular contexts than wound healing of breast epithelial cells, since these three genes did not score positive in our assay. Along with this idea, we found that PKN2 was translocating to cell-cell junctions of MCF10A cells specifically when the jammed monolayer was mechanically unjammed by the wound.

Similarly, we were able to unambiguously ascribe the phenotype of MOB4 KO cells, i.e. activation of collective migration and swirling, to defective YAP1 activation, since constitutively active YAP1 rescued both aspects of the MOB4 KO phenotype (Fig.8). Yet all three remaining proteins were also YAP1 regulators. DLG5 inhibits YAP1 [47]. TP53BP2 directly binds to YAP1 [64] and is required for its activation [65,66]. AMOTL2, like other motin family proteins, regulates YAP1 signaling in complex ways, in part by sequestering YAP1 at cell junctions [52,67]. In our system, however, only MOB4 controls collective cell migration and it does so through YAP1 activation in cells facing the wound.

MOB4 is a non-canonical regulator of YAP1 activity. There are several possible ways by which MOB4 can control YAP1 activation. MOB4 is a subunit of the striatin-interacting phosphatase and kinase (STRIPAK) complex, a multiprotein complex that contains the PP2A phosphatase [50] ; in addition to the phosphatase, MOB4 can recruit the MST4 kinase [48]. PP2A phosphatase activity

regulates the canonical activity of the essential MST1 kinase through its phosphatase activity [68]. Furthermore, the MOB4-MSTK4 complex can exchange subunits with the MOB1-MST1 complex and thus alternates between YAP activating and inactivating complexes [48]. A recently recognized level of YAP1 regulation involves the formation of distinct biomolecular condensates that can coalesce and mix their signaling components, adding further complexity to the signaling pathway [69]. Whatever the exact mechanism involved, the YAP1 activator role of MOB4 appears conserved in evolution, since the *C. elegans* MOB4 ortholog controls the life span of the model worm through YAP1 activation [70].

One of the most remarkable results of our work is that the two hits we identified interact with different domains of the plasma membrane in epithelial cells. PKN2 interacts with lateral edges of collectively migrating cells, whereas MOB4 interact with their front edge. Both PKN2 and MOB4 are cytosolic in the jammed epithelium and relocalize to their respective edge when the monolayer is mechanically unjammed by the wound. Their behavior is thus opposite to the one of NF2, which decorates the whole belt of adherens junctions when cells are jammed and relocalizes to the cytosol upon unjamming [24]. Since PKN2 and MOB4 both interact with the WAVE complex in their respective domain, they can be specific markers of protrusions involved in affixing the membranes of neighboring cells or translocating the cell forward, respectively. MOB4 appears more enriched at the front of follower cells than at the front of leader cells. Yet the role of MOB4 is not restricted to follower cells, since its inactivation also prevents YAP1 activation in leader cells.

MOB4 inactivation results in an overall increase of collective migration and the disorientation of collective migration. It is striking that YAP1 activation, and probably the target genes it induces, rescue the swirling behavior, in addition to the hyper-active collective migration. Indeed, since MOB4 is localized in such a way that it can indicate the migration orientation, it is surprising that one of the YAP1 target genes can indicate where to migrate, in the absence of MOB4. A more parsimonious hypothesis might be that MOB4 is a localized YAP1 inhibitor, in a manner analogous to Arpin, which inhibits the Arp2/3 at the lamellipodial edge, thus allowing cells to turn [71]. Along with this idea, swirling would be related to unrestrained collective cell migration. Since collective migration of MOB4 KO cells is unrestrained even in follower cells far from the wound, it is possible that these cells are too far to receive the orientation signal from leader cells immediately facing the wound.

Our work provides two novel molecular entry points into a complex and finely regulated process. The localization, function and mechanism of both PKN2 and MOB4 in collective cell migration were characterized in detail as much as we could. But these results also raise important questions for future studies. How are different membrane domains specified at the front and on the lateral sides of follower cells, which have neighboring cells all around? How is the orientation signal transmitted from the wound? How is it attenuated from one cell to the next? Which YAP1 target genes restrict collective migration? And how do they perform this function away from the wound, while being mostly expressed in cells facing the wound?

4. EXPERIMENTAL SECTION

Cells

MCF10A cells were a kind gift of Dr. Thierry Dubois, who organizes a collection of mammary epithelial cells of Institut Curie (Paris). They were cultured in DMEM/F12 medium (Gibco) supplemented with 5% horse serum (Sigma), 100 ng/mL cholera toxin (Sigma), 20 ng/mL epidermal growth factor (Sigma), 0.01 mg/mL insulin (Sigma), 500 ng/mL hydrocortisone (Sigma) and 100 U/mL penicillin/streptomycin (Gibco).

Plasmids and Isolation of Stable Cell Lines

The ORFs of PKN2 and MOB4 were amplified from MCF10A cDNA using RNA Plus (Macherey-Nagel) and SuperScript™ III Reverse Transcriptase (ThermoFisher Scientific) Kits. Both cDNAs were cloned into a custom MXS AAVS1L SA2A Puro bGHpA EF1 Flag EGFP Blue SV40pA AAVS1R vector using FseI and AscI restriction sites flanking Blue cassette. The pQCXIH-Myc-YAP-5SA plasmid encoding constitutively active Myc-tagged YAP1 (Uniprot entry P46937-2) comprising the 5 serine to alanine substitutions S61A, S109A, S127A, S164A, and S381A was a gift from Kun-Liang Guan (Addgene plasmid #33093). To obtain stable cell lines, cells were transfected with Lipofectamine 3000 (ThermoFisher Scientific), then diluted and selected with either 1 µg/ml of Puromycin (PKN2 and MOB4) or 15 µg/ml of Hygromycin (YAP1). Individual clones were picked up using cloning rings, expanded and analyzed by Western blot.

Generation of KO Cell Lines

gRNA sequences were selected in Genome Browser (https://genome-euro.ucsc.edu) based on the best on/off-targeting ratio. Four gRNAs per gene were chosen and their cleavage efficiency was assessed using the T7E1 assay [72] , the most efficient pair at inducing a genomic deletion between the two gRNAs was chosen. Oligonucleotides encoding the corresponding gRNA sequences were then cloned into the pRG2-GG vector at the BsaI restriction site. The gRNA sequences used for each gene were the following: PKN2 gRNA#1 5'-TTGGAGTATCTGGAGTCCTT-3', PKN2 gRNA#2 5'-GTATTCAAATGGATCTTCAA-3'; TP53BP2 gRNA#1 5'-TCGCCTCTATAAGGAGCTGC-3', TP53BP2 gRNA#2 5'-CAGCTAGAGATGCTCAAGAA-3'; DLG5 gRNA#1 5'-TTCCACAGGCACTACCGGGA-3', DLG5 gRNA#2 5'-CAATTACTACCTCTTGTCAA-3'; AMOTL2 gRNA#1, 5'-GGGGGACCGAGATCCCCGTG-3', AMOTL2 gRNA#2 5'-GGAGCTGCCCACCTATGAGG-3'; MOB4 gRNA#1 5'-AAATGTTTCATTCTGTAGAG-3', MOB4 gRNA#2 5'-CACATGCTTATTTTCATCAT-3'; gRNA ATP1A1 5'-GTTCCTCTTCTGTAGCAGCT-3'. Efficiency of each cloned gRNA was confirmed by the T7E1 DNA mismatch assay. To amplify the corresponding genomic regions encompassing Cas9-mediated DSBs, the following primer pairs were used: PKN2 for 5'- TCGAACTCAGCTGGAAACAA -3', PKN2 rev 5'- TTTTTGCATGAATTGGTTGAA -3'; TP53BP2 for 5'- GGAAGAAGGTGAGACCAGACC -3', TP53BP2 rev 5'- GCACCTGTAACCCCAGCTAC -3'; DLG5 for 5'- CATCTGTGAAAGGGGAATGC -3', DLG5 rev 5'- GCATTTCTGGACATGAGGTG -3'; AMOTL2 for, 5'- GTACTGAGGTGGGGGTCCTC -3', AMOTL2 rev 5'- CTGGAACTGGGGGTACAGG -3'; MOB4 for 5'- TCGCTTATTTTCCCTAGGTGTC -3', MOB4 rev 5'- CCCTTCATGCTTCACTTTCC -3'. To generate KO

lines, cells were cotransfected with 2 specific gRNA sequences with the plasmids expressing G2 targeting the *ATP1A1* gene and the one encoding Cas9, using Lipofectamine 3000 (ThermoFischer Scientific). After 3 days, cells were selected with 0.5 µM ouabain for 5 days. Individual clones were picked after 2 weeks of selection using cloning cylinders. To obtain a control cell line, in addition to parental cells, a stable pool of MCF10A cells resistant to ouabain, with no other genome alteration, was prepared. The genome of potentially KO clones was characterized by PCR using the previously indicated primers. The PCR product was sequenced using Sanger sequencing. If both alleles had the same mutation, the sequence of the PCR product was easily read. In case of overlapping signals in the sequencing chromatogram, the PCR product was cloned into the Zero Blunt vector (ThermoFischer Scientific) and clones corresponding to individual alleles were sequenced.

Antibodies

The following commercial antibodies were used: DLG5 (ThermoFisher Scientific #A302-302A-M), PKN2 (Proteintech #14608-1-AP), AMOTL2 (Proteintech #23351-1-AP), TP53BP2 (Proteintech #26550-1-AP), MOB4 (Proteintech #15886-1-AP), E-cadherin (clone DECMA-1, Sigma-Aldrich #MABT26), CYFIP2 (Sigma-Aldrich #SAB2701081), NCKAP1 (Bethyl Laboratories, A305-178A), Abi1 (ThermoFischer Scientific #PA5-78705), YAP1 (clone 63.7, SantaCruz Biotechnology #sc-101199), phospho-YAP1 (Ser127) (Proteintech #80694-2-RR, PtgLab), phospho-YAP1 (Ser397) (Proteintech #29018-1-AP), GFP (clones 13.1 and 7.1, Sigma-Aldrich #11814460001), Tubulin (clone DM1A, Sigma-Aldrich #T9026), $p150^{Glued}$/DCTN1 (BD Biosciences #BD610474), ERM proteins (Transduction Laboratories #M36820) phospho-Ezrin (Thr567)/Radixin (Thr564)/Moesin (Thr558) (Cell Signaling Technology #3726), GAPDH (ThermoFisher Scientific #AM4300). The following home-made rabbit polyclonal antibodies were used: Myc, WAVE2 and CYFIP1 [73].

Western Blots

Cell lysis was performed in 50 mM Hepes, pH7.7, 150 mM NaCl, 1 mM $CaCl_2$, 1% NP40, 0.5% Na Deoxycholate, and 0.1% SDS supplemented with protease and phosphatase inhibitor cocktails (Roche). Lysates were centrifuged at 20000 x g at 4°C, supernatants were mixed with LDS loading buffer (ThermoFischer Scientific) and 2.5% of β-ME. SDS-PAGE was performed using NuPAGE 4–12% Bis-Tris gels (ThermoFischer Scientific), proteins were transferred to a nitrocellulose membrane. Membranes were then blocked in 5% skimmed milk, incubated with primary and secondary antibodies. Secondary antibodies used were conjugated with either alkaline phosphatase (Promega) or with horse radish peroxidase (Sigma-Aldrich). Membranes were developed by using either NBT/BCIP as substrates (Promega) or with SuperSignal™ West Femto Maximum Sensitivity Substrate (ThermoFischer Scientific).

Immunofluorescence

Cells were seeded on glass coverslips previously coated with 20 µg/mL bovine fibronectin (Sigma) for 1 h at 37°C. Cells were fixed either in sparse culture or jammed or after 8 hours of collective migration depending on the experimental conditions in PBS/3.2% PFA then quenched with 50 mM

NH_4Cl, permeabilised with 0.5 % Triton X-100, blocked in 2% BSA and incubated with antibodies (1-5 µg/mL for the primary, 5 µg/mL for the secondary) or 1:3000 diluted SiR-actin (Tebu-bio). Secondary goat antibodies conjugated with Alexa Fluor 488, 555 or 647 or DAPI were from Life Technologies/ThermoFischer Scientific. Images were acquired using an inverted Axio Observer microscope (Zeiss) equipped with a 63×/1.4 oil objective, a mercury lamp, and a Hamamatsu camera C10600 Orca-R2 or a SP8ST-WS confocal microscope (Leica) equipped with a HC PL APO 63x/1.40 oil immersion objective, a white light laser, HyD and PMT detectors.

Immunoprecipitation

Cells expressing GFP fusion proteins were lysed with XB-NP40 buffer (50 mM HEPES, 50 mM KCl, 1% NP-40, 10 mM EDTA, pH7.7) supplemented with protease inhibitors during 30 min on ice. Clarified cell extracts were incubated with GFP-trap beads (Chromotek) for 1 h at 4 °C. The GFP-trap beads were washed with XB-NP40 buffer. Beads were subjected to SDS–PAGE and Western blot.

Wound Healing

For wound healing experiments, 80 000 cells were seeded in a Ibidi insert (Ibidi, 80209) and allowed to adhere for a 24 h. Wound was created by removing the insert. Cells were washed with fresh medium and imaged using videomicroscopy. Time-lapse multi-field experiments were performed in phase contrast or in GFP/mCherry fluorescent channels on automated inverted microscopes (Olympus IX71 or Zeiss AxioObserver Zeiss) both equipped with thermal and CO_2 regulation. Acquisitions were performed using a charge-coupled device (CCD) camera (Retiga 4000 R, QImaging or Hamamatsu camera C10600 Orca-R2) and Metamorph (Universal Imaging) or Micro Manager (ImageJ) software to control them. Images were taken every 10 min.

Phase contrast movies were analyzed using particle image velocimetry (PIV) performed in the PIVlab software package [74] for Matlab (MathWorks). To obtain the field of displacement vectors, the window size was set to 32 pixels = 23.75 µm with a 0.75 overlap. Spurious vectors were filtered out by their amplitude and replaced by interpolated velocity from neighboring vectors. A time sliding window averaging velocity fields over 40 minutes (4 frames) was used. Subsequent analysis was performed as previously described [57] using the published code to extract the order parameter and cell speed.

Force Measurement Using E-cadherin Coated Beads

We employed a procedure that we had previously set up [59]. In brief, experiments were conducted using an inverted epifluorescence microscope (Olympus Live EZ) equipped with a 40× objective (LUCPLFLN; NA/0.6) and an Andor Neo 5.5 CMOS (2560 x 2160px). The cells were seeded in a chamber composed of a U-shaped PDMS structure with two glass coverslips—one on top and one at the bottom. The bottom coverslip was coated with fibronectin to facilitate cell growth. Amine Dynabeads M270 (ThermoFischer Scientific #14307D) were conjugated with purified E-cadherin extracellular domain (SinoBiological #10204-H02H). Elastic micropipettes were created by pulling

them (Sutter P-97 micropipette puller) and cutting them with a homemade microforge to achieve an inner dimension of 2-3 µm. The micropipette was hold by a micropipette holder attached to a micromanipulator (Sutter MP-285), and the system was connected to a hydraulic setup to control bead capture through aspiration. The micropipette was maneuvered to contact the cell edge and gently pushed towards the cell with a displacement of 1-2 µm. Subsequently, the micropipette was gradually withdrawn from the cell by moving the chamber's stage in 3 µm increments at an average speed of 5 µm/s until detachment occurred. The bending deflection of the micropipette (x) was recorded, and the micropipette stiffness (k) was determined following calibration with a standard micropipette. The detachment force was calculated using the formula $F = kx$. Mean force values after 5 minutes of contact were derived from the results of more than 10 cells in each group, obtained from at least three independent experiments.

Statistics

Statistical analyses were carried out with GraphPad Prism software (v7.00) and Microsoft Excel 2016. Shapiro-Wilk normality test was applied to examine whether data fit a normal distribution. If data satisfied the normality criterion, ANOVA was followed by a post-hoc Tukey's multiple comparison test. If not, a non-parametric Kruskal-Wallis test was followed by a post-hoc Dunn's multiple comparison test. Pairwise comparisons were assessed by either the t-test if data followed a normal distribution or by the Mann-Whitney test otherwise. Four levels of significance were distinguished: * $p<0.05$, ** $p<0.01$, *** $p<0.001$, **** $p<0.0001$.

Author Contributions

A.I.F. performed most experiments and data analysis in the two research groups of P.S. and A.M.G. Y.L. performed force measurements using E-cadherin-coated beads. D.Y.G. adapted the ouabain selection procedure to the double cut approach for fast selection of KO cell lines. AIF and DYG isolated and characterized KO cell lines. H.Y.C. helped with PIV and analysis of wound healing; J.J. helped with data analysis; J.Y., P.S. and A.M.G. supervised the study in their respective research group. AIF and AMG jointly wrote the manuscript.

Conflict of interest

The authors declare no conflict of interest

Supporting Information

Supplementary information is available.

Data Availability

The data that support the findings of this study are available in the supplementary information.

Acknowledgements

This work was supported by grants from Agence Nationale de la Recherche (ANR-20-CE13-0016 to PS and AMG, ANR-22-CE13-0041 and ANR-24-CE44-4957 to AMG), Fondation ARC pour la Recherche sur le Cancer (ARC PJA 2021 060003815 to AMG). This work benefited from the support of the Personalized reconstitution of the tumoral process program led by l'X, Ecole polytechnique and the Fondation de l'Ecole polytechnique, sponsored by Servier. We thank the Polytechnique Bioimaging Facility for confocal microscopy partly supported by Agence Nationale de la Recherche (ANR-11-EQPX-0029 Morphoscope2, ANR-10-INBS-04 France BioImaging). Work in Institut Curie received support from the Labex Cell(n)Scales (grants ANR-11-LABX-0038, ANR-10-IDEX-0001-02), and received support from "Institut Pierre-Gilles de Gennes" laboratoire d'excellence, "Investissements d'avenir" program ANR-10-IDEX-0001-02 PSL and ANR-10-LABX-31, from Canceropôle Ile-de-France and French National Cancer Institute. We thank the Cell and Tissue Imaging core facility (PICT IBiSA), Institut Curie, member of the French National Research Infrastructure France-BioImaging (ANR10-INBS-04) and the Molecular Biology and Cellular Biology platform of CNRS UMR168. This study was supported by the Single-cell mechanical study was supported by National Research Foundation (NRF) Singapore, Mechanobiology Institute under its MID-SIZED GRANT (MSG) (NRF-MSG-2023-0001 to J.Y.). We thank Kun-Liang Guan (UCSD, CA) for the kind gift of the YAP1 plasmid.

REFERENCES

[1] R. Mayor, S. Etienne-Manneville, *Nat. Rev. Mol. Cell Biol.* **2016**, *17*, 97.

[2] P. Friedl, J. Locker, E. Sahai, J. E. Segall, *Nat. Cell Biol.* **2012**, *14*, 777.

[3] R. H. Insall, L. M. Machesky, *Developmental Cell* **2009**, *17*, 310.

[4] A. J. Ridley, *Cell* **2011**, *145*, 1012.

[5] R. Farooqui, G. Fenteany, *Journal of Cell Science* **2004**, *118*, 51.

[6] D. Krndija, F. E. Marjou, B. Guirao, S. Richon, O. Leroy, Y. Bellaiche, E. Hannezo, D. M. Vignjevic, *Science* **2019**, *365*, 705.

[7] M. Ozawa, S. Hiver, T. Yamamoto, T. Shibata, S. Upadhyayula, Y. Mimori-Kiyosue, M. Takeichi, *J. Cell Biology* **2020**, *219*, e202006196.

[8] L. Menin, J. Weber, S. Villa, E. Martini, E. Maspero, C. A. Niño, V. Cancila, A. Poli, P. Maiuri, A. Palamidessi, E. Frittoli, F. Bianchi, C. Tripodo, K. J. Walters, F. Giavazzi, G. Scita, S. Polo, *Cell Rep.* **2023**, *42*, 113001.

[9] C. Wu, S. B. Asokan, M. E. Berginski, E. M. Haynes, N. E. Sharpless, J. D. Griffith, S. M. Gomez, J. E. Bear, *Cell* **2012**, *148*, 973.

[10] P. Suraneni, B. Rubinstein, J. R. Unruh, M. Durnin, D. Hanein, R. Li, *The Journal of Cell Biology* **2012**, *197*, 239.

[11] S. Verma, A. M. Shewan, J. A. Scott, F. M. Helwani, N. R. den Elzen, H. Miki, T. Takenawa, A. S. Yap, *The Journal of biological chemistry* **2004**, *279*, 34062.

[12] N. K. Lee, K. W. Fok, A. White, N. H. Wilson, C. J. O'Leary, H. L. Cox, M. Michael, A. S. Yap, H. M. Cooper, *Nature communications* **2016**, *7*, 11082.

[13] J. X. H. Li, V. W. Tang, K. A. Boateng, W. M. Brieher, *Proc. National Acad. Sci.* **2021**, *118*, e2023510118.

[14] J. X. H. Li, V. W. Tang, W. M. Brieher, *Proceedings of the National Academy of Sciences of the United States of America* **2020**, *117*, 432.

[15] N. Efimova, T. M. Svitkina, *J Cell Biol* **2018**, *217*, 1827.

[16] S. Verma, S. P. Han, M. Michael, G. A. Gomez, Z. Yang, R. D. Teasdale, A. Ratheesh, E. M. Kovacs, R. G. Ali, A. S. Yap, *Molecular Biology of the Cell* **2012**, *23*, 4601.

[17] D. Yamazaki, T. Oikawa, T. Takenawa, T. Takenawa, *Journal of Cell Science* **2007**, *120*, 86.

[18] B. Ladoux, R.-M. Mège, *Nat. Rev. Mol. Cell Biol.* **2017**, *18*, 743.

[19] P. Friedl, R. Mayor, *Cold Spring Harb. Perspect. Biol.* **2017**, *9*, a029199.

[20] S. Garcia, E. Hannezo, J. Elgeti, J.-F. Joanny, P. Silberzan, N. S. Gov, *Proceedings of the National Academy of Sciences of the United States of America* **2015**, *112*, 15314.

[21] C. Malinverno, S. Corallino, F. Giavazzi, M. Bergert, Q. Li, M. Leoni, A. Disanza, E. Frittoli, A. Oldani, E. Martini, T. Lendenmann, G. Deflorian, G. V. Beznoussenko, D. Poulikakos, K. H. Ong, M. Uroz, X. Trepat, D. Parazzoli, P. Maiuri, W. Yu, A. Ferrari, R. Cerbino, G. Scita, *Nature materials* **2017**, *16*, 587.

[22] D. Cai, S.-C. Chen, M. Prasad, L. He, X. Wang, V. Choesmel-Cadamuro, J. K. Sawyer, G. Danuser, D. J. Montell, *Cell* **2014**, *157*, 1146.

[23] J. L. Bays, K. A. DeMali, *Cellular and Molecular Life Sciences* **2017**, *74*, 2999.

[24] T. Das, K. Safferling, S. Rausch, N. Grabe, H. Boehm, J. P. Spatz, *Nature Cell Biology* **2015**, *17*, 276.

[25] K. T. Furukawa, K. Yamashita, N. Sakurai, S. Ohno, *Cell Rep.* **2017**, *20*, 1435.

[26] T. Panciera, L. Azzolin, M. Cordenonsi, S. Piccolo, *Nature Reviews Mol Cell Biol* **2017**, *18*, 758.

[27] J. Park, D.-H. Kim, S. R. Shah, H.-N. Kim, Kshitiz, D. Ellison, P. Kim, K.-Y. Suh, A. Quiñones-Hinojosa, A. Levchenko, *Nat. Commun.* **2019**, *10*, 2797.

[28] D. Kim, J. M. Olson, J. A. Cooper, *J. Cell Biol.* **2024**, *223*, e202401057.

[29] A. Tsherniak, F. Vazquez, P. G. Montgomery, B. A. Weir, G. Kryukov, G. S. Cowley, S. Gill, W. F. Harrington, S. Pantel, J. M. Krill-Burger, R. M. Meyers, L. Ali, A. Goodale, Y. Lee, G. Jiang, J. Hsiao, W. F. J. Gerath, S. Howell, E. Merkel, M. Ghandi, L. A. Garraway, D. E. Root, T. R. Golub, J. S. Boehm, W. C. Hahn, *Cell* **2017**, *170*, 564.

[30] K. A. DeMali, C. A. Barlow, K. Burridge, *The Journal of Cell Biology* **2002**, *159*, 881.

[31] J. James, A. I. Fokin, D. Y. Guschin, H. Wang, A. Polesskaya, S. N. Rubtsova, C. L. Clainche, P. Silberzan, A. M. Gautreau, S. Romero, *Life Sci. Alliance* **2025**, *8*, e202402583.

[32] E. E. Bosco, Y. Nakai, R. F. Hennigan, N. Ratner, Y. Zheng, *Oncogene* **2010**, *29*, 2540.

[33] A. S. Mohan, K. M. Dean, T. Isogai, S. Y. Kasitinon, V. S. Murali, P. Roudot, A. Groisman, D. K. Reed, E. S. Welf, S. J. Han, J. Noh, G. Danuser, *Developmental Cell* **2019**, *49*, 444.

[34] B. Serrels, A. Serrels, V. G. Brunton, M. Holt, G. W. McLean, C. H. Gray, G. E. Jones, M. C. Frame, *Nature Cell Biology* **2007**, *9*, 1046.

[35] R. T. Böttcher, M. Veelders, P. Rombaut, J. Faix, M. Theodosiou, T. E. Stradal, K. Rottner, R. Zent, F. Herzog, R. Fässler, *The Journal of Cell Biology* **2017**, *113*, jcb. 201701176.

[36] S. Romero, C. L. Clainche, A. M. Gautreau, *Biochemical Journal* **2020**, *477*, 1.

[37] S. Vincent, J. Settleman, *Molecular and Cellular Biology* **1997**, *17*, 2247.

[38] S. W. Wallace, A. Magalhaes, A. Hall, *Molecular and Cellular Biology* **2010**, *31*, 81.

[39] Z. Guo, L. J. Neilson, H. Zhong, P. S. Murray, S. Zanivan, R. Zaidel-Bar, *Science Signaling* **2014**, *7*, rs7.

[40] Y. Wang, F. Bu, C. Royer, S. Serres, J. R. Larkin, M. S. Soto, N. R. Sibson, V. Salter, F. Fritzsche, C. Turnquist, S. Koch, J. Zak, S. Zhong, G. Wu, A. Liang, P. A. Olofsen, H. Moch, D. C. Hancock, J. Downward, R. D. Goldin, J. Zhao, X. Tong, Y. Guo, X. Lu, *Nature Cell Biology* **2014**, *16*, 1092.

[41] R. F. Hennigan, J. S. Fletcher, S. Guard, N. Ratner, *Science Signaling* **2019**, *12*, eaau8749.

[42] T. Wu, H. Song, D. Xie, B. Zhao, H. Xu, C. Wu, K. Hua, Y. Deng, C. Ji, J. Hu, L. Fang, *International journal of oncology* **2018**, 1.

[43] C. Royer, E. Sandham, E. Slee, F. Schneider, C. B. Lagerholm, J. Godwin, N. Veits, H. Hathrell, F. Zhou, K. Leonavicius, J. Garratt, T. Narendra, A. Vincent, C. Jones, T. Child, K. Coward, C. Graham, M. Fritzsche, X. Lu, S. Srinivas, *Nat. Commun.* **2022**, *13*, 941.

[44] M. Wakabayashi, T. Ito, M. Mitsushima, S. Aizawa, K. Ueda, T. Amachi, N. Kioka, *The Journal of biological chemistry* **2003**, *278*, 21709.

[45] T. Nechiporuk, T. E. Fernandez, V. Vasioukhin, *Dev. Cell* **2007**, *13*, 338.

[46] T. Sezaki, K. Inada, T. Sogabe, K. Kakuda, L. Tomiyama, Y. Matsuno, T. Ichikawa, M. Matsuo, K. Ueda, N. Kioka, *PLoS ONE* **2012**, *7*, e35519.

[47] J. Liu, J. Li, P. Li, Y. Wang, Z. Liang, Y. Jiang, J. Li, C. Feng, R. Wang, H. Chen, C. Zhou, J. Zhang, J. Yang, P. Liu, *Sci Rep* **2017**, *7*, 42125.

[48] M. Chen, H. Zhang, Z. Shi, Y. Li, X. Zhang, Z. Gao, L. Zhou, J. Ma, Q. Xu, J. Guan, Y. Cheng, S. Jiao, Z. Zhou, *The Journal of biological chemistry* **2018**, *293*, 14455.

[49] C. S. Moreno, W. S. Lane, D. C. Pallas, *The Journal of biological chemistry* **2001**, *276*, 24253.

[50] B.-C. Jeong, S. J. Bae, L. Ni, X. Zhang, X. Bai, X. Luo, *Nat. Struct. Mol. Biol.* **2021**, *28*, 290.

[51] S. Moleirinho, W. Guerrant, J. L. Kissil, *FEBS Letters* **2014**, *588*, 2693.

[52] P. Amirifar, J. Kissil, *Oncogene* **2023**, *42*, 1265.

[53] C. Yi, S. Troutman, D. Fera, A. Stemmer-Rachamimov, J. L. Avila, N. Christian, N. L. Persson, A. Shimono, D. W. Speicher, R. Marmorstein, L. Holmgren, J. L. Kissil, *Cancer Cell* **2011**, *19*, 527.

[54] D. Agudelo, A. Duringer, L. Bozoyan, C. C. Huard, S. Carter, J. Loehr, D. Synodinou, M. Drouin, J. Salsman, G. Dellaire, J. Laganière, Y. Doyon, *Nat Methods* **2017**, *14*, 615.

[55] N. Molinie, A. Gautreau, *Methods in molecular biology (Clifton, N.J.)* **2018**, *1749*, 11.

[56] M. Poujade, E. Grasland-Mongrain, A. Hertzog, J. Jouanneau, P. Chavrier, B. Ladoux, A. Buguin, P. Silberzan, *Proceedings of the National Academy of Sciences* **2007**, *104*, 15988.

[57] M. Deforet, M. C. Parrini, L. Petitjean, M. Biondini, A. Buguin, J. Camonis, P. Silberzan, *Nature Methods* **2012**, *9*, 1081.

[58] L. Petitjean, M. Reffay, E. Grasland-Mongrain, M. Poujade, B. Ladoux, A. Buguin, P. Silberzan, *Biophys. J.* **2010**, *98*, 1790.

[59] W. Huang, C. Fu, J. Yan, *Methods Mol. Biol.* **2023**, *2600*, 267.

[60] B. Zhao, X. Wei, W. Li, R. S. Udan, Q. Yang, J. Kim, J. Xie, T. Ikenoue, J. Yu, L. Li, P. Zheng, K. Ye, A. Chinnaiyan, G. Halder, Z.-C. Lai, K.-L. Guan, *Genes Dev.* **2007**, *21*, 2747.

[61] F.-X. Yu, B. Zhao, N. Panupinthu, J. L. Jewell, I. Lian, L. H. Wang, J. Zhao, H. Yuan, K. Tumaneng, H. Li, X.-D. Fu, G. B. Mills, K.-L. Guan, *Cell* **2012**, *150*, 780.

[62] K. J. Simpson, L. M. Selfors, J. Bui, A. Reynolds, D. Leake, A. Khvorova, J. S. Brugge, *Nature Cell Biology* **2008**, *10*, 1027.

[63] S. Hildebrand, S. Hultin, A. Subramani, S. Petropoulos, Y. Zhang, X. Cao, J. Mpindi, O. Kalloniemi, S. Johansson, A. Majumdar, F. Lanner, L. Holmgren, *Sci. Rep.* **2017**, *7*, 9540.

[64] X. Espanel, M. Sudol, *J. Biol. Chem.* **2001**, *276*, 14514.

[65] C. Royer, S. Koch, X. Qin, J. Zak, L. Buti, E. Dudziec, S. Zhong, I. Ratnayaka, S. Srinivas, X. Lu, *PLoS ONE* **2014**, *9*, e111384.

[66] T. Konno, T. Kohno, T. Okada, H. Shimada, S. Satohisa, S. Kikuchi, T. Saito, T. Kojima, *Histochem. Cell Biol.* **2020**, *154*, 197.

[67] B. Zhao, L. Li, Q. Lu, L. H. Wang, C.-Y. Liu, Q. Lei, K.-L. Guan, *Genes Dev.* **2011**, *25*, 51.

[68] Y. Zheng, B. Liu, L. Wang, H. Lei, K. D. P. Prieto, D. Pan, *Cell Rep.* **2017**, *21*, 3612.

[69] L. Wang, K. Choi, T. Su, B. Li, X. Wu, R. Zhang, J. H. Driskill, H. Li, H. Lei, P. Guo, E. H. Chen, Y. Zheng, D. Pan, *Cell* **2022**, *185*, 4376.

[70] M. Jahan, H. Iwasa, H. Kuroyanagi, Y. Hata, *Genes Cells* **2021**, *26*, 798.

[71] I. Dang, R. Gorelik, C. Sousa-Blin, E. Derivery, C. Guérin, J. Linkner, M. Nemethova, J. G. Dumortier, F. A. Giger, T. A. Chipysheva, V. D. Ermilova, S. Vacher, V. Campanacci, I. Herrada, A.-G. Planson, S. Fetics, V. Henriot, V. David, K. Oguievetskaia, G. Lakisic, F. Pierre, A. Steffen, A. Boyreau, N. Peyriéras, K. Rottner, S. Zinn-Justin, J. Cherfils, I. Bièche, A. Y. Alexandrova, N. B. David, J. V. Small, J. Faix, L. Blanchoin, A. Gautreau, *Nature* **2013**, *503*, 281.

[72] D. Y. Guschin, A. J. Waite, G. E. Katibah, J. C. Miller, M. C. Holmes, E. J. Rebar, *Methods Mol. Biol.* **2010**, *649*, 247.

[73] A. Gautreau, H. H. Ho, J. Li, H. Steen, S. P. Gygi, M. W. Kirschner, *Proceedings of the National Academy of Sciences of the United States of America* **2004**, *101*, 4379.

[74] W. Thielicke, R. Sonntag, *J. Open Res. Softw.* **2021**, *9*, 12.

A **Dependency maps**

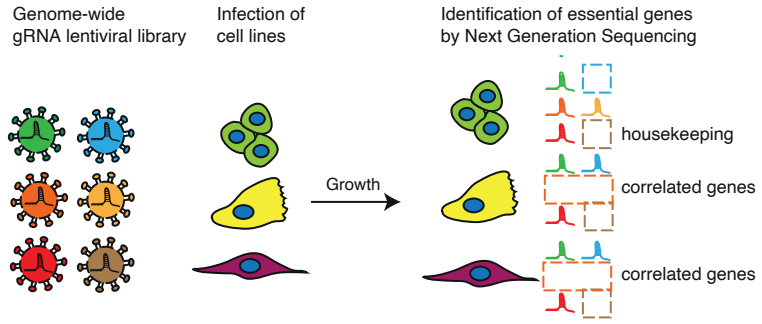

B **Correlations**

	RWA Mechanosensing					Candidate Genes				
GENE	*RAC1*	*NCKAP1*	*ARPC4*	*NF2*	*VCL*	*PKN2*	*TP53BP2*	*DLG5*	*MOB4*	*AMOTL2*
AMOTL2	-0.35	-0.28	-0.29	0.62	-0.30	-0.40	-0.28	-0.36	-0.29	1.00
MOB4	0.42	0.36	0.39	-0.32		0.40	0.31		1.00	
DLG5	0.35	0.36	0.30	-0.39	0.26	0.43	0.25	1.00		
TP53BP2	0.32	0.36	0.34	-0.35	0.32	0.46	1.00			
PKN2	0.45	0.42	0.39	-0.45	0.39	1.00				
VCL	0.44	0.43		-0.33	1.00					
NF2	-0.35	-0.32	-0.30	1.00						
ARPC4	0.45	0.46	1.00							
NCKAP1	0.53	1.00								
RAC1	1.00									

C **Isolation of KO cell lines**

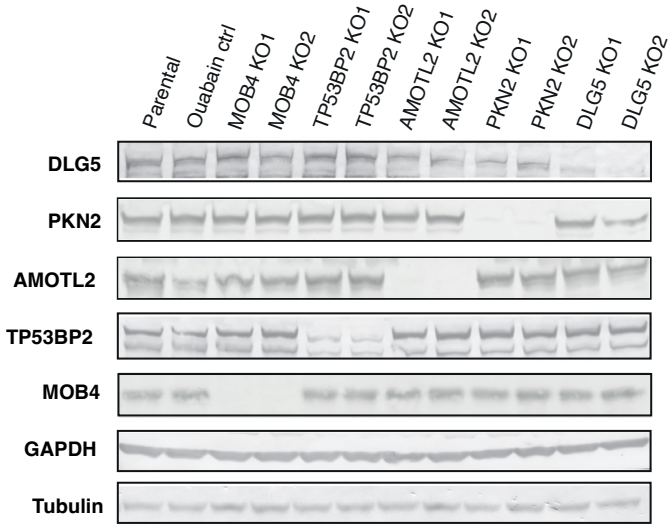

Figure 1. Loss-of-function of candidate genes and identification of *PKN2* and *MOB4* that regulate collective cell migration. A) Dependency maps reveal essential genes in more than 500 cell lines. Genes that are required in the same subset of lines are correlated and may function in the same pathway. B) Matrix reporting gene correlations between known genes of the mechanosensing RAC1-WAVE-Arp2/3 pathway (RWA) and five new candidate genes associated with cell-cell junctions. C) Knock-Out (KO) of the five candidate genes was obtained in the MCF10A breast epithelial cell line. Two independent clones of each KO were analyzed by Western blots using the indicated antibodies.

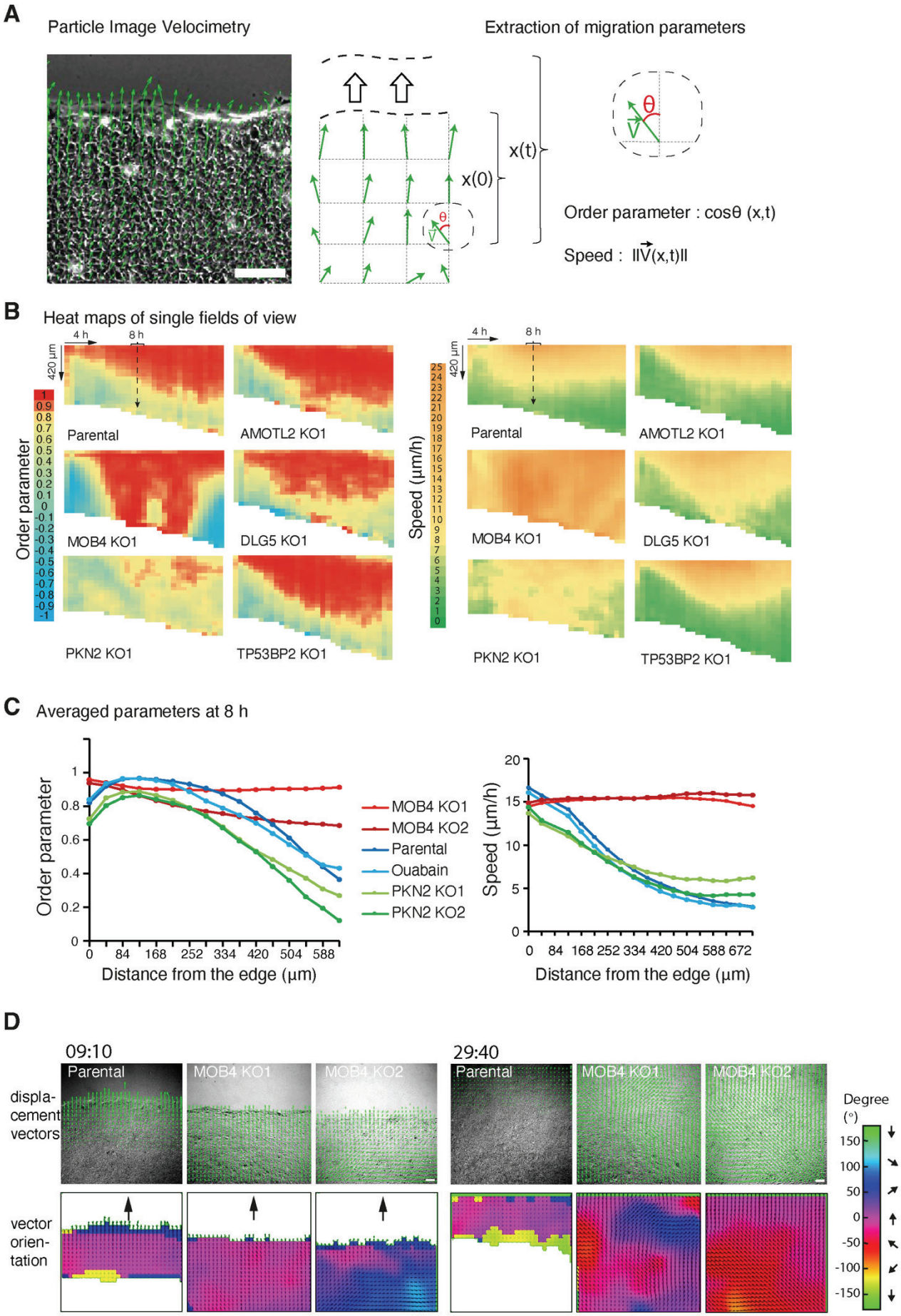
A
Particle Image Velocimetry
Extraction of migration parameters
x(t)
x(0)
θ
Order parameter : cosθ (x,t)
Speed : ||V(x,t)||
B
Heat maps of single fields of view
4 h
8 h
420 µm
Order parameter
Speed (µm/h)
Parental
AMOTL2 KO1
MOB4 KO1
DLG5 KO1
PKN2 KO1
TP53BP2 KO1
C
Averaged parameters at 8 h
Order parameter
Distance from the edge (µm)
MOB4 KO1
MOB4 KO2
Parental
Ouabain
PKN2 KO1
PKN2 KO2
Speed (µm/h)
Distance from the edge (µm)
D
09:10
29:40
Parental
MOB4 KO1
MOB4 KO2
displa-
cement
vectors
vector
orien-
tation
Degree
(°)

Figure 2. identification of *PKN2* and *MOB4* as genes that controls the coordination of collective cell migration. A) the field of displacement vectors are obtained by Particle Image Velocimetry (PIV) of wound healing movies and superimposed to phase contrast images of MCF10A monolayers after wounding. Scale bar: 100 µm. B) Order parameter and speed are extracted from the field of displacement vectors and plotted as heat maps across time and space. This heat map representation shows the monolayer front facing the wound on top and time 0 on the left. For one KO clone of each candidate gene, heat maps of one movie representative of 12 are plotted. Three independent experiments gave the same result. The dashed line represents the time 8 h. C) Local order and absolute velocity are averaged at 8 h after wounding from the 12 fields of view of the three biological repeats. Front-rear gradients of the local order are altered in PKN2 and MOB4 KO cells. PKN2 KO strongly impairs order, revealing that migration of PKN2 KO cells is not coordinated, while MOB4 KO induces robust swirling collective migration, indicated by enhanced speed, but with an orientation that is not stably directed toward the wound over time. D) Angular distribution of displacement vectors. Displacement vectors obtained by PIV are superimposed with phase contrast images. Time in h:min after wounding.

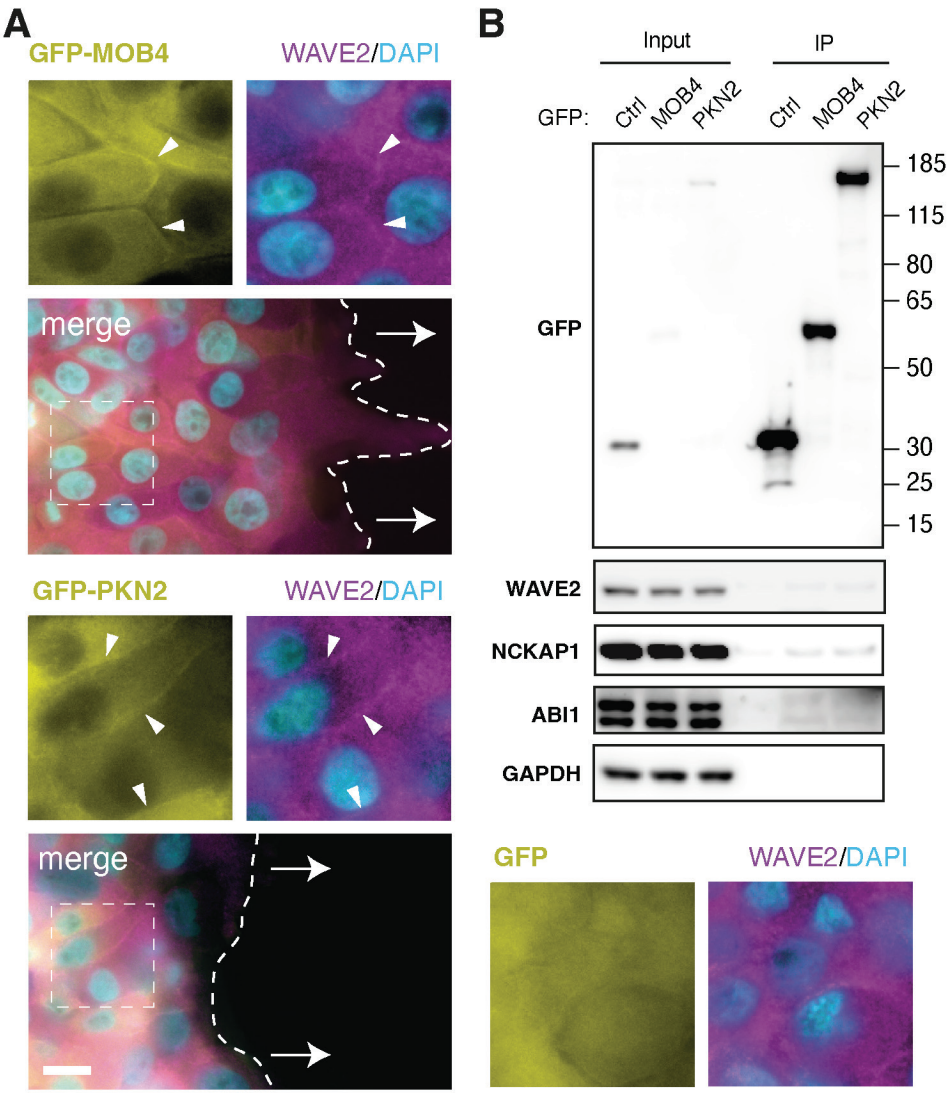

Figure 3. Both MOB4 and PKN2 associate with the WAVE complex at cell-cell junctions. A) Both PKN2 and MOB4 co-localize with WAVE2 during collective cell migration, 8 h after wounding. Still images extracted from wide-field videomicroscopy, scale bar 20 µm. B) Immunoprecipitation of GFP-tagged MOB4, PKN2, or GFP as a control. The WAVE complex co-precipitates with both MOB4 and PKN2. One experiment representative of three is shown.

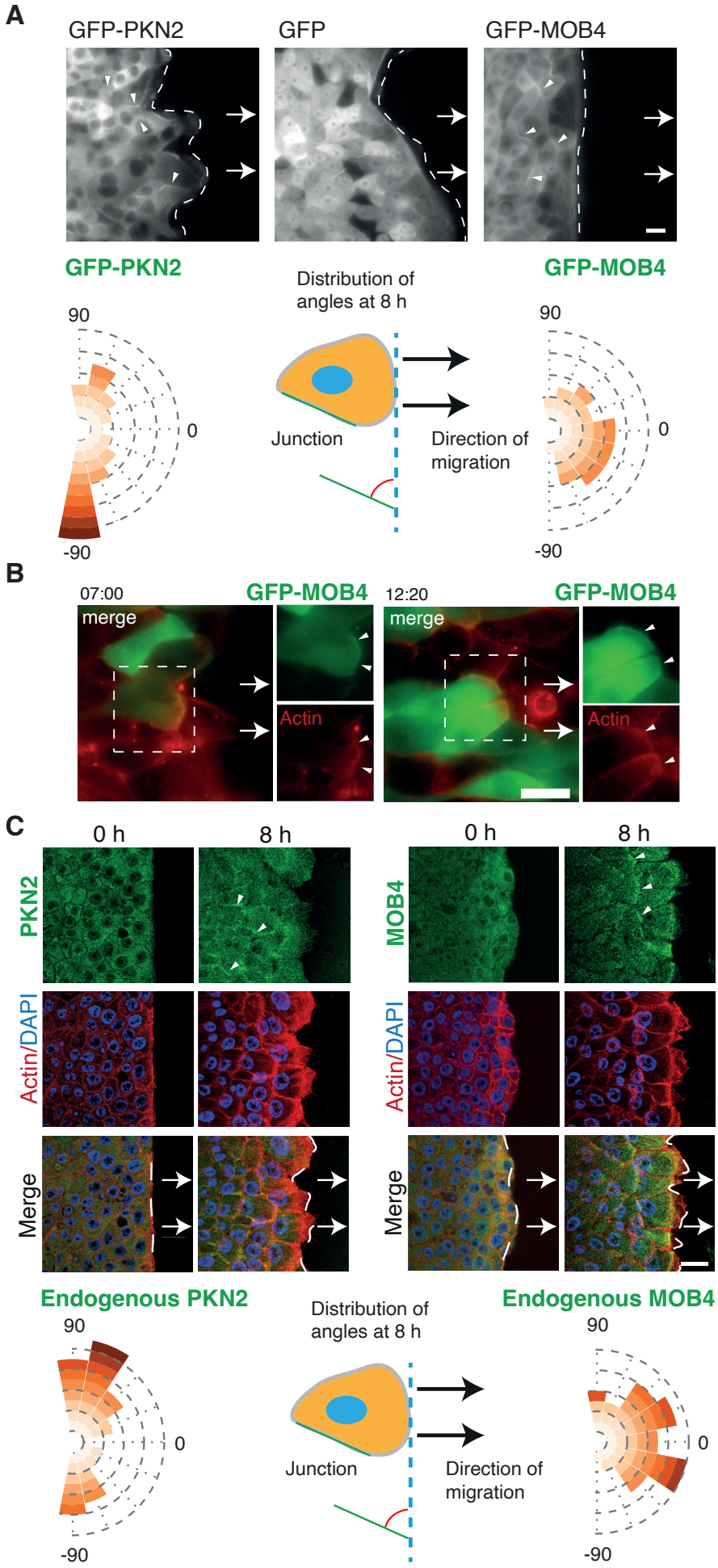
A
GFP-PKN2
GFP
GFP-MOB4
GFP-PKN2
Distribution of angles at 8 h
GFP-MOB4
90
0
-90
Junction
Direction of migration
90
0
-90
B
07:00
GFP-MOB4
merge
Actin
12:20
GFP-MOB4
merge
Actin
C
0 h
8 h
0 h
8 h
PKN2
MOB4
Actin/DAPI
Actin/DAPI
Merge
Merge
Endogenous PKN2
Distribution of angles at 8 h
Endogenous MOB4
90
0
-90
Junction
Direction of migration
90
0
-90

Figure 4. PKN2 and MOB4 differentially localize to front and lateral edges of collectively migrating cells. A) Stable MCF10A lines expressing GFP-PKN2 or GFP-MOB4 are imaged by wide-field microscopy. Enrichment of PKN2 on the lateral sides of follower cells and enrichment of MOB4 parallel to the wound edge during wound healing. Angle distribution of cell junctions labelled by MOB4 or PKN2. In total, more than 200 junctions per cell line are assessed in two independent experiments. B) A mixed population of GFP-MOB4 expressing and non-fluorescent parental MCF10A cells reveal that MOB4 is enriched at the front, and not at the rear, of collectively migrating cell. Still images extracted from wide-field videomicroscopy. C) PKN2 and MOB4 immunofluorescence in MCF10A monolayers at time 0 or 8 h after wounding. Filamentous actin is stained with phalloidin and nuclei with DAPI. Confocal microscopy. Angle distribution of cell junctions labelled by MOB4 or PKN2. More than 50 junctions for each staining are assessed in two independent experiments. Scale bars 20 µm.

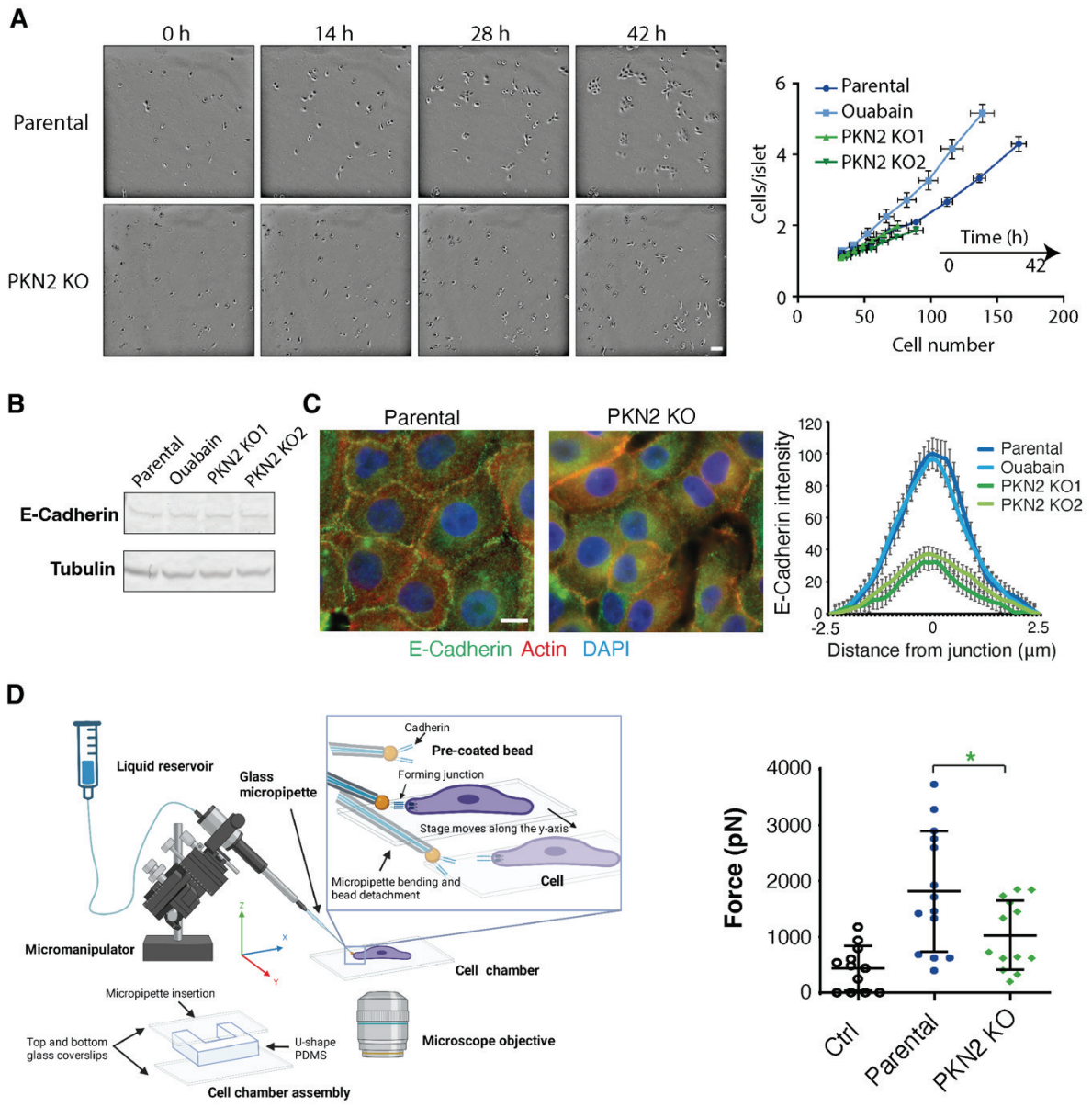

Figure 5. PKN2 KO cells display weakened adherens junctions. A) Growth of single cell populations of PKN2 KO and control cell lines over time. Number of cells per islet is plotted as a function of cell number. Five movies are analyzed per condition, two independent experiments gave similar results. For the plot, data were pooled from the total of n=10 fields of view. Scale bar: 100 µm. B) Western blot of E-cadherin or tubulin as a loading control. C) E-cadherin immunofluorescence in PKN2 KO and control cells at subconfluency. Filamentous actin is stained with phalloidin and nuclei with DAPI. Scale bar 10 µm. Two independent experiments gave similar results. Intensity profiles, taken perpendicularly to cell-cell junctions were averaged for a total of n=40 junctions. Mean ± SD. D) Adhesion force measurements of E-cadherin coated beads to PKN2 KO and parental cells. CTRL refers to force measurement when beads are uncoated. The set-up used consists in a chamber composed of a U-shaped PDMS structure btween two glass coverslips, where cells are seeded and manipulated. The liquid reservoir, when placed below the plane of the cells, allows aspirating beads. When the micromanipulator is used to displace the bead, the micropipette bends because of bead attachment, until the bonds attaching the bead to the cell rupture. From the micropipette deflection, the force of the E-cadherin mediated bonds is calculated knowing the measured elasticity of the micropipette.

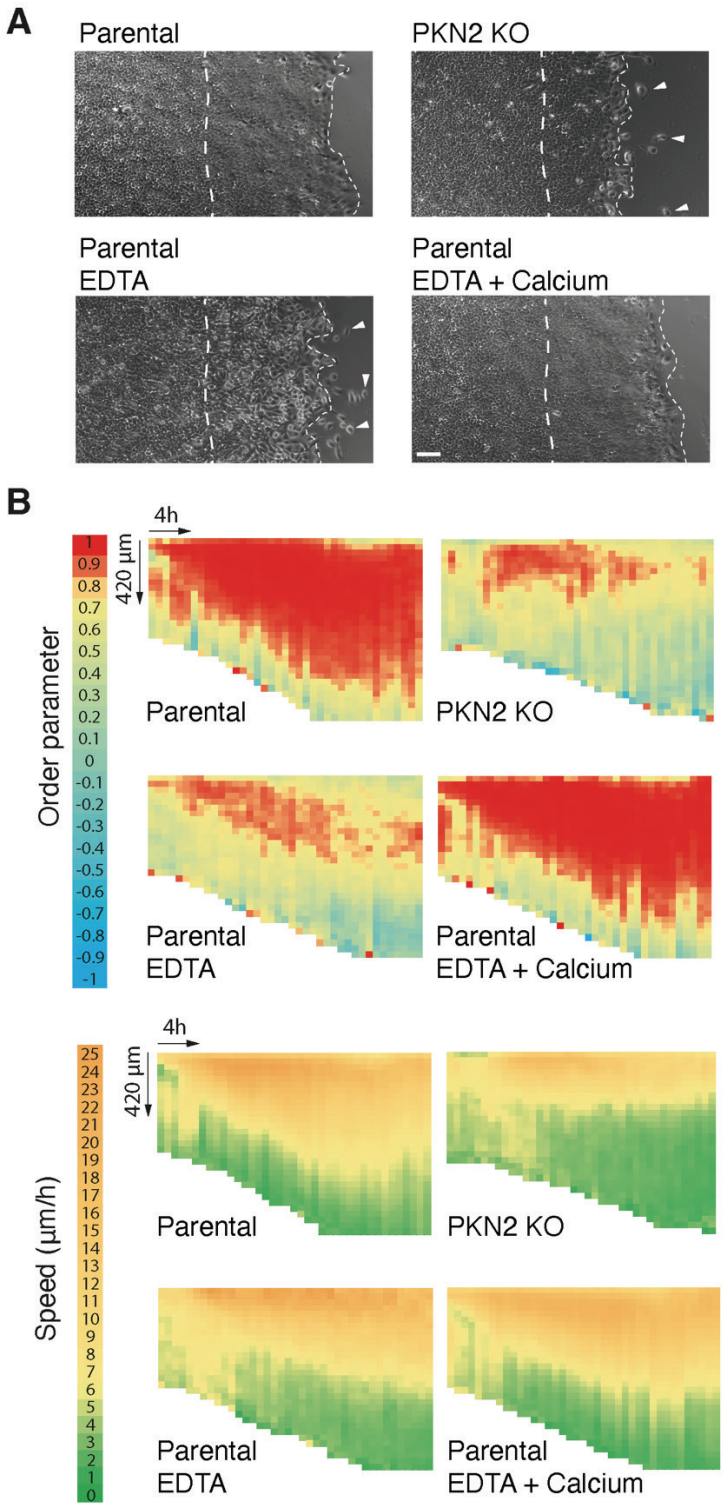

Figure 6. EDTA, which weakens adherens junctions, phenocopies PKN2 KO cells. A) Wound healing of PKN2 KO cells or parental cells treated with 1 mM EDTA to destabilize cell-cell junctions or 1 mM EDTA with 1 mM $CaCl_2$ to restore E-cadherin homotypic binding. Cells that dissociate from the edge are indicated by arrowheads. EDTA-mediated destabilization of junctions phenocopies the PKN2 KO phenotype. Scale bar 100 µm. B) Heat maps of local order and absolute velocities extracted from PIV analyses of 12 movies per condition. Two independent experiments gave similar results.

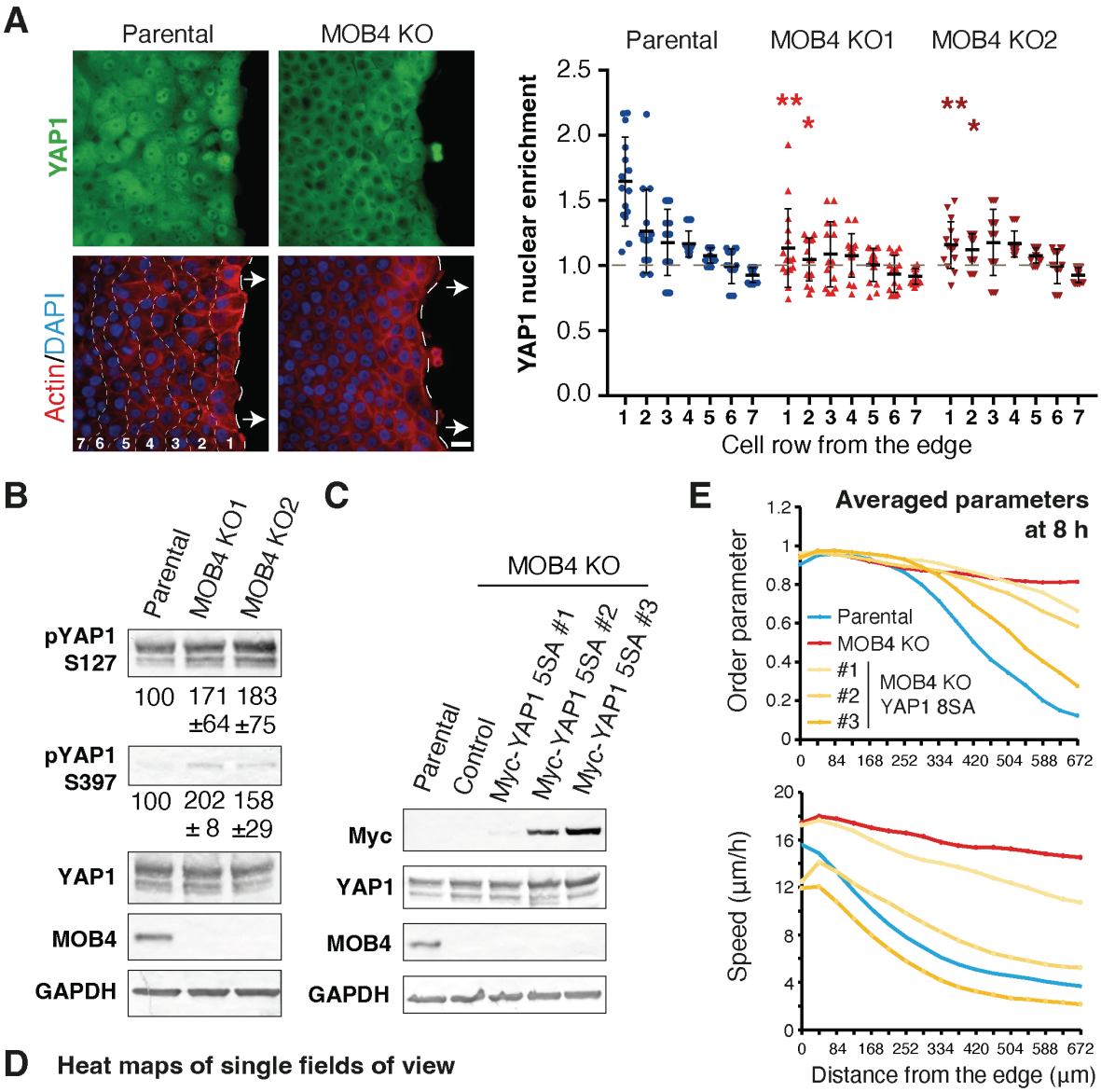
A
Parental
MOB4 KO
YAP1
Actin/DAPI
7 6 5 4 3 2 1
Parental
MOB4 KO1
MOB4 KO2
YAP1 nuclear enrichment
2.5
2.0
1.5
1.0
0.5
0.0
**
*
**
*
1 2 3 4 5 6 7 1 2 3 4 5 6 7 1 2 3 4 5 6 7
Cell row from the edge
B
Parental
MOB4 KO1
MOB4 KO2
pYAP1 S127
100 171 183
±64 ±75
pYAP1 S397
100 202 158
± 8 ±29
YAP1
MOB4
GAPDH
C
MOB4 KO
Parental
Control
Myc-YAP1 5SA #1
Myc-YAP1 5SA #2
Myc-YAP1 5SA #3
Myc
YAP1
MOB4
GAPDH
E
Averaged parameters at 8 h
Order parameter
1.2
1
0.8
0.6
0.4
0.2
0
Parental
MOB4 KO
#1
#2
#3
MOB4 KO YAP1 8SA
0 84 168 252 334 420 504 588 672
Speed (µm/h)
20
16
12
8
4
0
0 84 168 252 334 420 504 588 672
Distance from the edge (µm)
D
Heat maps of single fields of view
Order parameter
1 0.9 0.8 0.7 0.6 0.5 0.4 0.3 0.2 0.1 0 -0.1 -0.2 -0.3 -0.4 -0.5 -0.6 -0.7 -0.8 -0.9 -1
Speed (µm/h)
30 29 28 27 26 25 24 23 22 21 20 19 18 17 16 15 14 13 12 11 10 9 8 7 6 5 4 3 2 1 0
4 h
420 µm
Parental
MOB4 KO
MOB4 KO YAP1 5SA #1
MOB4 KO YAP1 5SA #2
MOB4 KO YAP1 5SA #3
4 h
420 µm
Parental
MOB4 KO
MOB4 KO YAP1 5SA #1
MOB4 KO YAP1 5SA #2
MOB4 KO YAP1 5SA #3

Figure 7. MOB4 regulates collective cell migration through YAP1 activation. A) YAP1 immunofluorescence, phalloidin and DAPI staining in MOB4 KO and parental cells, 8 h after wounding. Wide-field microscopy, scale bar: 20 µm. YAP1 nuclear enrichment is assessed in different rows of cells from the wound edge. Five fields of view are analyzed per condition. One-way ANOVA, * $p<0.05$, ** $p<0.01$. Three independent experiments gave similar results. YAP1 is enriched in the nucleus of parental cells in a gradient from the edge. In contrast, YAP1 is cytosolic throughout MOB4 KO monolayers. B) Western blots of YAP1 and phosphoYAP1 in MOB4 KO and parental cells. The ratio of phosphoYAP1 over YAP1 is indicated; mean ± SD of 3 independent measurement. C) The constitutively active mutant of YAP1, 8SA, is stably expressed in MOB4 KO cells. Myc Western blots reveal 3 clones with increasing expression of the YAP1 transgene. D) Constitutively active YAP1 rescues the swirling collective migration of MOB4 KO cells in a dose-dependent manner. Heat maps of local order and absolute velocity of single fields of view, representative of 15, are plotted. Three independent experiments gave the same result. E) Local order and absolute velocity are averaged at 8 h after wounding from the 15 fields of view of the three biological repeats.

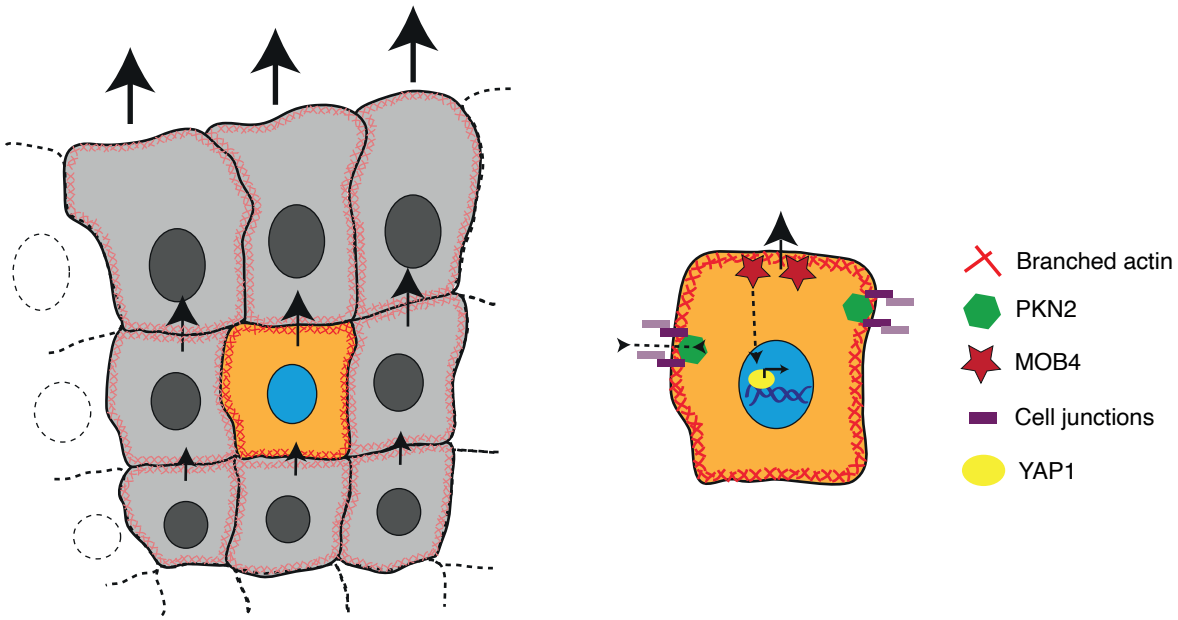

Figure 8. Working model of the roles of PKN2 and MOB4 in the control of collective cell migration. PKN2 localizes at lateral junctions and maintains cohesiveness of the cell monolayer through the maintenance of adherens junctions, whereas MOB4 localizes at the front edge and indicates the cell where to migrate through the expression of YAP1 target genes.